UNDER-SAMPLED FUNCTIONAL MRI USING LOW-RANK PLUS SPARSE MATRIX DECOMPOSITION

Vimal Singh[†] *Ahmed H. Tewfik*[†] *David B. Ress*[⋆]

[†] The University of Texas at Austin, Austin, Texas, USA
[⋆] Baylor College of Medicine, Houston, Texas, USA

ABSTRACT

High spatial resolution in functional magnetic resonance imaging improves its sensitivity to brain activation signals by reducing partial volume effects. However, the long acquisition times required for high spatial resolution limit the temporal resolution in fMRI studies. Consequently, the low temporal sampling bandwidth leads to increase in physiological noise and poor modeling of the functional activation dynamics. Thus, fast techniques capable of recovering fMRI time-series from under-sampled data are desirable to improve the sensitivity and specificity of fMRI for functional brain mapping. This paper presents an under-sampled fMRI recovery using low-rank plus sparse matrix decomposition signal model. This model is suited for blocked or slow event-related fMRI studies, where the low-rank matrix captures the temporally static T_2^*-weighted image patterns and, the sparse matrix captures the pseudo-periodic brain activation signal. The preliminary results of under-sampled recovery on in-vivo fMRI data show recovery of BOLD activation in human superior colliculus with contrast-to-noise ratio ≥ 4.4 (85% of reference) up to acceleration factors of 3.

***Index Terms*—** Magnetic resonance imaging, Compressed sensing, functional MRI, Low-rank methods, Sparse recovery

1. INTRODUCTION

Functional magnetic resonance imaging (fMRI) using blood oxygen level-dependent (BOLD) contrast is used for advancing fundamental understanding of the brain by measuring the hemodynamic correlates of neuronal activity [1, 2, 3, 4]. High spatial resolution fMRI is desirable as it provides greater localization of activation in the brain enabling identification of small functional-sub units, such as superior colliculs [3] and pulvinar nucleus of thalamus [4]. However, small voxel sizes concomitantly require long readout durations that are adversely affected by signal decay and off-resonance effects. As an alternative, segmented data acquisition schemes (multi-shot) are used with shorter readouts per segment (shot). However, segmented acquisitions are prone to subject-motion and respiration induced off-resonance effects. More importantly, both single- and multi-shot acquisitions limit the temporal resolution of the high spatial resolution fMRI studies. Low temporal sampling bandwidths result in aliasing of physiological noise which reduces the sensitivity of fMRI to BOLD signal [2, 5]. There is, therefore, a need for fMRI techniques that provide rapid single-shot imaging with short readout durations to reduce off-resonance artifacts while maintaining high spatial and temporal resolutions. This paper presents an fMRI technique based on modeling the spatio-temporal fMRI signal as a low-rank plus sparse matrix decomposition that allows for fMRI signal recovery from its under-sampled data.

In the past decade, many techniques based on the theory of compressed sensing (CS) have been proposed for accelerating various dynamic MRI applications, such as myocardial perfusion imaging [6, 7] and MR angiography [8, 9]. However, application of CS to fMRI has been limited and only few studies have been reported [10, 11, 12]. In [10], authors use the sparsity of images in wavelet transform domain in combination with variable density spiral acquisitions to achieve acceleration factors of 1.4. Exploiting the compressibility of images in the spatial domain only and ignoring the temporal redundancy in the fMRI signal results in low acceleration gains. In [12], multi-shot echo planar imaging (EPI) based under-sampling is combined with low-rank matrix completion to accelerate resting state fMRI studies. Similar to a sparse signal, which only has a few significant representation coefficients, a low-rank matrix only has few large singular values. The low-rank of a matrix signifies a low degree of freedom and is used to recover the matrix from its under-sampled version. In [12], each temporal frame is considered a column of a space-time matrix, where the spatio-temporal correlations produce a low-rank matrix [13, 14]. Using matrix completion, resting state fMRI studies were accelerated up to factors of 4.27 in [12]. However, for task based fMRI studies the assumption of low-rank matrix is too strong to capture the weak BOLD activation signals in addition to the relatively slow-evolving non-activation related functional brain networks.

This paper presents a fast fMRI technique based on recovery of $2d$-time images from under-sampled data using the low-rank plus sparse matrix decomposition model. The combination of low-rank model (LR) and the sparsity of signal representations (S) has been successfully applied to computer vision, where it enables separation of background from the foreground in a video sequence [15]. The (LR+S) decomposition is ideal for fMRI signals evoked by slowly varying experiments using blocked or slow event-related designs, where LR can model the temporally correlated background, and S can model the dynamic BOLD activity. In such experiments, the neural activation is limited to relatively small portion of the imaged volume. The time series of the activated voxels is pseudo-periodic as it is a convolution of a stereotypical hemodynamic response function with a periodic stimulus presentation (to invoke neural metabolism). Additionally, the non-activated volume voxels show non-task related activity which changes slowly over time. Thus, in the (LR+S) decomposition of fMRI signal, the LR can model the non-task related temporally correlated signal and the S can model the pseudo-periodic BOLD activity.In the proposed fMRI signal decomposition: 1) redundancy in both space and time are exploited unlike [10] and, 2) the additional S modeling of the BOLD activity improves its sensitivity over that of [12]. In this paper a preliminary evaluation of fMRI recovery using the (LR+S) model is done using phantom simulation and retrospective under-sampling of in-vivo fMRI data. The preliminary results show good signal recovery of superior colliculus

activation (conrast-to-noise ratio $\geq$ 4.4, 85% of reference signal) up to acceleration factors of R= 3.

The rest of this paper is organized as follows. Section 2 presents the low-rank plus sparse decomposition model for the fMRI signal. Section 3 presents the simulation and retrospective under-sampling experiments for fMRI data recovery. Finally, section 4 concludes the paper citing future direction.

2. METHOD

This section presents the mathematical formulation of the proposed fast fMRI technique. Section 2.1 details the low-rank plus sparse matrix (LR+S) decomposition for the fMRI signal. In section 2.2, the under-sampled fMRI recovery formulation based on the (LR+S) model is detailed.

2.1. Low-Rank Plus Sparse Matrix Decomposition

The time series of images in a fMRI data set is converted to a matrix $\mathbf{M}$ in which each column is a temporal frame. The low-rank plus sparse matrix approach aims to decompose the matrix $\mathbf{M}$ as a superposition of a low-rank matrix $\mathbf{L}$ (few non-zero singular values) and a sparse matrix $\mathbf{S}$ (few non-zero entries). The decomposition is unique and the problem is well posed if the low-rank component is not sparse, and vice versa if the sparse component does not have low rank [15, 16]. This condition is referred to as incoherence between $\mathbf{L}$ and $\mathbf{S}$. For example, these conditions are guaranteed if the singular vectors of $\mathbf{L}$ are not sparse and if the non-vanishing entries of $\mathbf{S}$ occur at random locations [16]. Low-rank matrix completion from under-sampled data is performed by minimizing the nuclear norm of the matrix (sum of singular values), which is the analog of the $l1$-norm for signal vectors (sum of absolute values) [17]. Therefore, the $\mathbf{L}+\mathbf{S}$ decomposition is performed by solving the following convex optimization problem:

$$\min \parallel \mathbf{L} \parallel_* + \lambda \parallel \mathbf{S} \parallel_1 \quad \text{s.t.} \quad \mathbf{M} = \mathbf{L} + \mathbf{S} \tag{1}$$

where, $\parallel \mathbf{L} \parallel_*$ is the nuclear norm of the matrix $\mathbf{L}$, $\parallel \mathbf{S} \parallel_1$ is the $l1$-norm of $\mathbf{S}$, and λ is a tuning parameter that balances the contribution of the $l1$-norm term relative to the nuclear norm term.

2.2. Under-Sampled fMRI Recovery

The $\mathbf{L}+\mathbf{S}$ decomposition given in eqn. (1) is modified to reconstruct under-sampled fMRI as follows:

$$\min \parallel \mathbf{L} \parallel_* + \lambda \parallel \mathbf{TS} \parallel_1 \quad \text{s.t.} \quad \mathbf{E}\,(\mathbf{L}+\mathbf{S}) = d \tag{2}$$

where, $\mathbf{T}$ is a sparsifying transform for $\mathbf{S}$, $\mathbf{E}$ is the encoding or acquisition operator, and d is the under-sampled data. $\mathbf{L}$ and $\mathbf{S}$ like $\mathbf{M}$ are defined as space-time matrices, where each column is a temporal frame; and d is a column vector. Note that $\mathbf{E}$ is a linear operator that maps the underlying fMRI time-series data to the under-sampled data vector d.

A version of eqn. 2 using regularization instead of strict constraints is formulated as follows:

$$\min_{\mathbf{L},\mathbf{S}} \frac{1}{2} \parallel \mathbf{E}(\mathbf{L}+\mathbf{S}) - d \parallel_2^2 + \mu \parallel \mathbf{L} \parallel_* + \lambda \parallel \mathbf{TS} \parallel_1 \tag{3}$$

where, the parameters trade μ and λ trade-off data consistency with complexity of the solution given by the sum of the nuclear- and $l1$-norm. In [18], the optimization problem in eqn. 3 is solved using iterative soft thresholding of the singular values of $\mathbf{L}$ and of the entries of $\mathbf{TS}$. Soft thresholding or shrinkage operator is defined as $\Lambda_\lambda(x) = \frac{x}{|x|}\max(|x| - \lambda, 0)$, in which x is a complex number and the threshold λ is real valued. This is extended to matrices by applying the shrinkage operation to each entry. Next, we define the singular value thresholding (SVT) by $SVT_\lambda = U\Lambda_\lambda(\Sigma)V^H$, where $\mathbf{M} = U\Sigma V^H$ is any singular value decomposition of $\mathbf{M}$. In the proposed $\mathbf{L}+\mathbf{S}$ reconstruction algorithm, in the k-th iteration the SVT operator is applied to $\mathbf{M}_{k-1} - \mathbf{S}_{k-1}$, then the shrinkage operator is applied to $\mathbf{M}_{k-1} - \mathbf{L}_{k-1}$ and the new $\mathbf{M}_k$ is obtained by enforcing data consistency, where the aliasing artifacts corresponding to the residual in k-space $\mathbf{E}^*(\mathbf{E}(\mathbf{L}_k + \mathbf{S}_k - d)$ are subtracted from $\mathbf{L}_k + \mathbf{S}_k$. Here $\mathbf{E}^*$ refers to the adjoint operator of $\mathbf{E}$, which maps a vector to a matrix. The algorithm iterates until the relative change in the solution is less than 10^{-5}, i.e., until $\parallel (\mathbf{L}_k + \mathbf{S}_k) - (\mathbf{L}_{k-1} + \mathbf{S}_{k-1}) \parallel_2 \leq 10^{-5} \parallel \mathbf{L}_{k-1} + \mathbf{S}_{k-1} \parallel_2$. This algorithm represents a combination of singular value thresholding used for matrix completion [17] and iterative soft thresholding used for sparse reconstruction.

3. EXPERIMENTS AND RESULTS

3.1. Phantom Simulations

This section presents under-sampled fMRI recovery using the (LR+S) signal decomposition on Shepp-Logan phantom based simulated data. Fig. 1a shows the Shepp-Logan phantom which is used to simulate a $2d$-time fMRI BOLD activation data. Based on the assumption that in task-based fMRI studies the functional activation is spatially restricted, modulation of time-series data is restricted to two ellipses shown with colored outlines in fig. 1a. Time-series for the two activation ellipses are obtained by convolving the commonly used double Gamma hemodynamic response function (HRF) with a blocked stimulus presentation time-curve [2]. A blocked stimulation period of 24 time-points is used with a 50% duty cycle. The simulated fMRI data matrix has a size of 512x512x96 for 4 functional activation cycles. For realistic simulations of fMRI data, electrical noise is added in the spatial Fourier space using a zero-mean Normal distribution to each sample at a signal-to-noise ratio of 20. In addition, to simulate weak activations, maximum amplitude modulation is restricted to 2% of the gray-scale intensity of the selected ellipses. The fMRI data is Fourier transformed and under-sampled using the variable density $2DFT$ technique [11]. The under-sampled data is then used to recover the complete fMRI time-series data based on the formulation of eqn. 3 using the algorithm summarized in sec. 2.2. Temporal Fourier transform is used as the sparsifying transform $\mathbf{T}$ in eqn. 3. The parameters $\mu = 0.01$ and $\lambda = 0.01$ are selected by trial-and-error for best signal recovery.

Figure 1 shows the results of under-sampled fMRI recovery on the simulated data at an acceleration of $R = 4$. Figure 1b shows a y-t plane (marked by the yellow-dashed line in fig. 1a) from the data. The y-t plane corresponds to the noisy ground truth ($\mathbf{M}$) and shows the temporal modulations within the activation ellipses. Figures 1c and 1d show the same y-t plane from the low-rank model $\mathbf{L}$ and the sparse matrix $\mathbf{S}$ recovered from the under-sampled data, respectively. The $\mathbf{L}$ time-series data within the activated-ellipses show negligible variations similar to those of the non-activated regions. In contrast, the $\mathbf{S}$ time-series captures the strong pseudo-periodic activation signal. Figure 1f shows a voxel time-series from the red-boundary-ellipse of fig. 1a. This plot shows the temporal-variations and the amplitude differences between the $\mathbf{L}$ and the $\mathbf{S}$ signals with respect to the noisy ground truth. As stated earlier, the $\mathbf{L}$ shows negligible temporal variations and the $\mathbf{S}$ aligns well with the BOLD

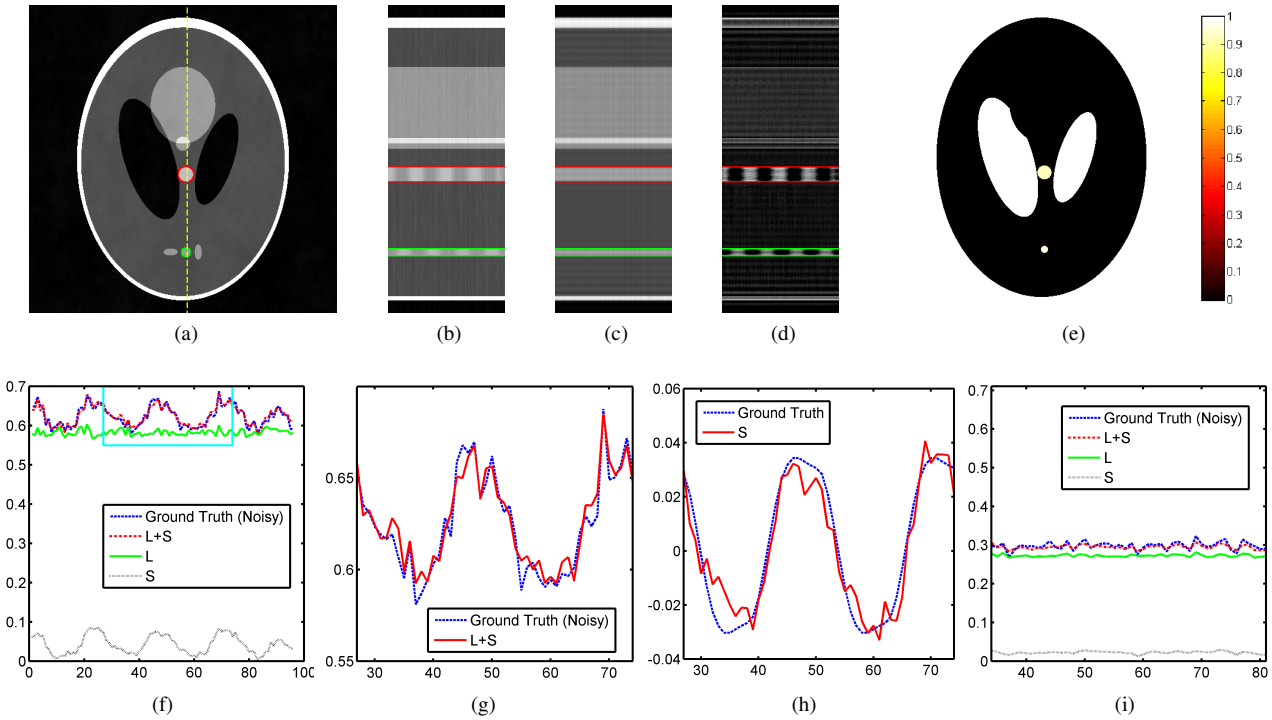

Fig. 1: Results of under-sampled recovery on a Shepp-Logan based simulated fMRI data-set at an acceleration of $R = 4$. (a) A Shepp-Logan time frame; (b) Simulated noisy y-t plane corresponding to the yellow line in (a); Recovered y-t plane from: (c) low-rank matrix $\mathbf{L}$, (d) sparse matrix $\mathbf{S}$; (e) Correlation map of sparse ($\mathbf{S}$) component of time-series with noise-free BOLD activation signal; Time-series of a voxel: (f), (g) & (h) belonging to red-outlined ellipse in (a), (i) a non-activated voxel.

activation signal. A zoomed-region (marked by cyan colored boundary) from fig. 1f containing 2 activation cycles is shown in figs. 1g and 1h. In fig. 1g, the recovered time-series ($\mathbf{L} + \mathbf{S}$, red-solid) follows the noisy ground truth data (blue-dashed) closely with a correlation of 0.96. Similarly, in fig. 1h, the recovered sparse component ($\mathbf{S}$, red-solid) follows the noise-free activation data (blue-dashed) closely with a correlation 0.95. In fig. 1h, the time-series curves are mean-shifted to zero to remove the dc offset between the two curves. Figure 1e shows the correlation of the sparse component $\mathbf{S}$ with the noise-free BOLD activation signal. The correlation coefficients for non-image regions are fixed to 1 for easier visualization. Clearly, the $\mathbf{S}$ shows high correlation only with the two activation ellipses: red: 0.93 ± 0.02 and green: 0.97 ± 0.02. Figure 1i shows the time-series curves for a non-activated voxel, for which the $\mathbf{S}$ time-series curve has very low amplitude and shows no inherent periodicity.

3.2. In-vivo fMRI Data

This section details the under-sampled fMRI recovery experiments on in-vivo data acquired on healthy volunteers. Imaging were performed on a Siemens 3T scanner using Archimedean spiral trajectories [19]. Acquisition parameters are selected to acquire a field-of-view of 192-mm at high spatial resolution of 1.2-mm using a 3-shot acquisition with a TR$=$ 1 sec/shot, i.e., one functional volume is acquired every 3 sec. The imaging planes are oriented to cover the superior colliculus (SC), a small laminar structure situated on the rostral surface of the brainstem. The SC is functionally associated with visual attention and occulomotor responses [20]. To invoke the functional response in SC, subjects perform a lateralized stimulation and attention task based on a speed discrimination of moving dots during image acquisition [20]. To evaluate the performance of an under-sampled fMRI recovery technique its sensitivity to BOLD activation will be quantified and compared with that of a standard fMRI acquisition. The BOLD sensitivity is measured in terms of functional-contrast-to-noise (fCNR) ratio. To extract fCNR within a region-of-interest (ROI) in a fMRI time-series, a sinusoid at the stimulus presentation frequency is fit to the normalized time series at each voxel, and from this fit, volume maps of response amplitude, coherence, and phase are derived. The amplitude quantifies the BOLD activation, while the phase measures the time-lag between stimulus onset and the hemodynamic response. The coherence value is equivalent to the correlation coefficient of the time-series data with its best-fit sinusoid. The mean amplitude within the ROI is used as the functional contrast. To measure the noise, bootstrapping was used to estimate confidence intervals on the functional contrast obtained in each session. Experiments runs within session were resampled with replacement, and the resampled set was then averaged and analyzed to obtain the functional contrast. This process was repeated 10^4 times to generate a statistical distribution of the contrast. The 68% confidence intervals were calculated from this distribution, and our noise level was defined as half the difference between the upper and lower interval. For a normal noise distribution, this calculation would precisely correspond to the standard-error-of-the-mean.

The in-vivo data is under-sampled by reducing the number of spiral shots used for reconstruction and also shifting from Archimedean to variable-density spiral trajectories [21]. However, the variable-density parameters (r, α in eq. (1) in [21]) are selected to keep the #sample/shot identical to that used for acquiring the fMRI data. Thus, for the 3-shot spiral acquisition, acceleration

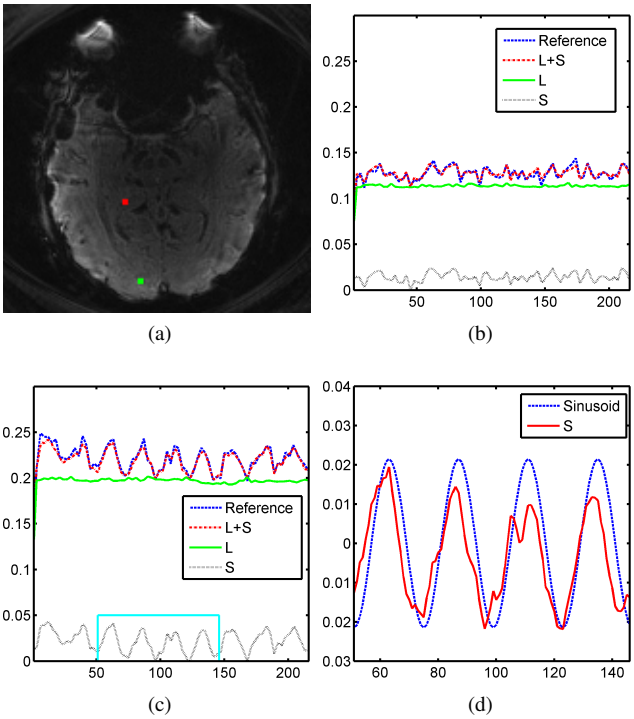

Fig. 2: Results of under-sampled fMRI recovery on in-vivo data at an acceleration of R= 3. (a) A sample recovered fMRI image; Time-series: (b) of a non-activated voxel (red in (a)), (c) of an activated voxel in visual cortex (green in (a)); (d) Sparse component with a sinusoid at the stimulus frequency with correlation = 0.84.

factors of R= 1.67 and R= 3 are possible. For under-sampled recovery using eqn. 3, the encoding operator $\mathbf{E}$ and its adjoint ($\mathbf{E}^*$) are derived using the NUFFT toolbox [22]. Figure 2 shows results for under-sampled recovery at acceleration of R= 3 with $\mu = 0.005$ and $\lambda = 0.001$ selected empirically to yield the best recovery performance. Figure 2a shows a recovered fMRI image in which two different voxels are marked. The red voxel is in non-activated brain region and its time-series are shown in fig. 2b. The green voxel lies in the visual cortex and its time series are shown in fig. 2c. Similar to phantom results, the sparse component captures the pseudo-periodic BOLD activity and the low-rank matrix component captures the temporally correlated data. Fig. 2d shows the $\mathbf{S}$ component for green voxel which shows high coherence (0.84) with a sinusoid at the stimulus frequency (also shown).

Table 1: FCNR in superior colliculus for under-sampled fMRI recovered time-series data at various accelerations (R).

Recovery Method	R= 1.67	R= 3
Wavelet sparsity [10]	3.7 ± 0.7	2.8 ± 0.6
Low-rank model [12]	4.6 ± 0.5	4.2 ± 0.4
Proposed (LR+S) model	4.9 ± 0.4	4.4 ± 0.5

Figure 3 shows the results of BOLD activation analysis in the superior colliculus (SC) for the under-sampled recovery at R= 3 and compares with that of the reference data (no under-sampling). Fig-

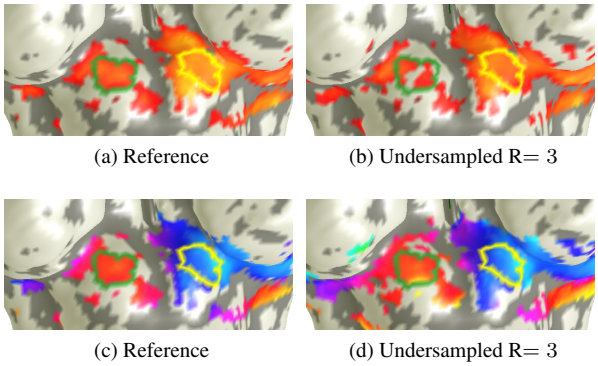

Fig. 3: Comparison of BOLD activation analysis on superior colliculus for an under-sampled recovery at acceleration of $R = 3$. Top-row: Coherence maps, Bottom-row:Phase maps

ures 3a and 3b show the coherence values for BOLD activation for the reference (0.50 ± 0.06) and the under-sampled data (0.46 ± 0.07), respectively. The coherence values are overlaid on a 3D segmentation of the brainstem and the outlines delineate the left- (green) and right-SC (yellow) ROIs. These ROIs are used to calculate the fCNR (later reported) which is used for quantitative evaluation of the BOLD sensitivity of the fMRI recovery technique. In figs. 3a and 3b, the coherence maps are threshold-ed below at 0.39, i.e., all transparent regions have coherence values smaller than 0.39. The under-sampled data shows slightly weaker activations which can be attributed to smoothing of data due to the constraint of sparsity in the temporal Fourier domain. Figures 3c and 3d compare the phase distributions of the activation signals in the reference and under-sampled data, respectively. Minor differences in phase distributions are observed for the left SC and changes are negligible in the right SC. For statistically relevant quantification of the proposed fast fMRI technique, retrospective under-sampling experiments are repeated on 3 healthy volunteers for the SC activation task. Table 1 summarizes the (mean $\pm$ std.) fCNR in SC ROIs for the proposed technique and the approaches of [10] and [12]. Functional CNR for reference fMRI data for 3 subjects is 5.2 ± 0.6. From table 1 for all techniques, with increasing acceleration the fCNR decreases, however, the decrease is minimum for the proposed (LR+S) model. The proposed fMRI technique: 1) does significantly better than the approach of [10] which does not model the temporal redundancies in the fMRI signal and, 2) marginally outperforms than the approach of [12] as the sparse S component is more appropriate for modeling the BOLD activity. In addition, for the proposed technique and [12], prospective under-sampling should further improve BOLD sensitivity by reducing physiological noise due to a real increase in temporal sampling bandwidth as opposed to in retrospective under-sampling experiments.

4. CONCLUSIONS

This paper presents an under-sampled fMRI recovery technique using the low-rank plus sparse matrix decomposition model. In task based fMRI, the low-rank matrix models the temporally correlated resting-state signal and the sparse component models the pesudo-periodic BOLD activity. The preliminary results on in-vivo fMRI data show recovery of activation signals with contrast-to-noise ratio $\geq$ 4.4 (85% of reference signal) up to accelerations R= 3.

5. REFERENCES

[1] S. Ogawa, D. W. Tank, R. Menon, J. M. Ellermann, S. G. Kim, H. Merkle, and K. Ugurbil, "Intrinsic signal changes accompanying sensory stimulation: Functional brain mapping with magnetic resonance imaging," *Proceedings of the National Academy of Sciences*, vol. 89, no. 13, pp. 5951–5955, July 1992.

[2] N.K. Logothetis and J. Pfeuffer, "On the nature of the {BOLD} fmri contrast mechanism," *Magnetic Resonance Imaging*, vol. 22, no. 10, pp. 1517 – 1531, 2004, Proceedings of the International School on Magnetic Resonance and Brain Function Frontiers of Brain Functional {MRI} and Electrophysiological Methods Proceedings of the International School on Magnetic Resonance and Brain Function.

[3] D. Ress, G.H. Glover, J. Liu, and B. Wandell, "Laminar profiles of functional activity in the human brain," *NeuroImage*, vol. 34, no. 1, pp. 74 – 84, 2007.

[4] D. A. Feinberg and E. Yacoub, "The rapid development of high speed, resolution and precision in fMRI," *NeuroImage*, vol. 62, no. 2, pp. 720–725, Aug. 2012.

[5] L. R. Frank, R. B. Buxton, and E. C. Wong, "Estimation of respiration-induced noise fluctuations from undersampled multislice fMRI data," *Magnetic Resonance in Medicine*, vol. 45, no. 4, pp. 635–644, Apr. 2001.

[6] G. Adluru, C. McGann, P. Speier, E.G. Kholmovski, A. Shaaban, and E.V.R. DiBella, "Acquisition and reconstruction of undersampled radial data for myocardial perfusion magnetic resonance imaging," *Journal of Magnetic Resonance Imaging*, vol. 29, no. 2, pp. 466–473, 2009.

[7] L. Ge, A. Kino, M. Griswold, C.A. Mistretta, J.C. Carr, and D. Li, "Myocardial perfusion MRI with sliding-window conjugate-gradient HYPR," *Magnetic Resonance in Medicine*, vol. 62, no. 4, pp. 835–839, 2009.

[8] C. A. Mistretta, O. Wieben, J. Velikina, W. Block, J. Perry, Y. Wu, K. Johnson, and Y. Wu, "Highly constrained backprojection for time-resolved MRI," *Magnetic Resonance in Medicine*, vol. 55, no. 1, pp. 30–40, 2006.

[9] C.A. Mistretta, "Undersampled radial MR acquisition and highly constrained back projection (HYPR) reconstruction: Potential medical imaging applications in the post-Nyquist era," *Journal of Magnetic Resonance Imaging*, vol. 29, no. 3, pp. 501–516, 2009.

[10] D. J. Holland, C. Liu, X. Song, E. L. Mazerolle, M. T. Stevens, A. J. Sederman, L. F. Gladden, R. C. N. D'Arcy, C. V. Bowen, and S. D. Beyea, "Compressed sensing reconstruction improves sensitivity of variable density spiral fMRI," *Magnetic Resonance in Medicine*, pp. n/a – n/a, 2013.

[11] X. Zong, J. Lee, A. J. Poplawsky, S. G. Kim, and J. C. Ye, "Compressed sensing fmri using gradient-recalled echo and {EPI} sequences," *NeuroImage*, vol. 92, no. 0, pp. 312 – 321, 2014.

[12] M. Chiew, S. M. Smith, P. J. Koopmans, N. N. Graedel, T. Blumensath, and K. L. Miller, "k-t FASTER: Acceleration of functional MRI data acquisition using low rank constraints," *Magnetic Resonance in Medicine*, pp. n/a–n/a, Aug. 2014.

[13] Z. Liang, "Spatiotemporal imagingwith partially separable functions," in *Biomedical Imaging: From Nano to Macro, 2007. ISBI 2007. 4th IEEE International Symposium on*, April 2007, pp. 988–991.

[14] J.P. Haldar and Z. Liang, "Spatiotemporal imaging with partially separable functions: A matrix recovery approach," in *Biomedical Imaging: From Nano to Macro, 2010 IEEE International Symposium on*, April 2010, pp. 716–719.

[15] V. Chandrasekaran, S. Sanghavi, P. Parrilo, and A. Willsky, "Rank-sparsity incoherence for matrix decomposition," *SIAM Journal on Optimization*, vol. 21, no. 2, pp. 572–596, 2011.

[16] E. J. Candès, X. Li, Y. Ma, and J. Wright, "Robust principal component analysis?," *J. ACM*, vol. 58, no. 3, pp. 11:1–11:37, June 2011.

[17] J. Cai, E. Candes, and Z. Shen, "A singular value thresholding algorithm for matrix completion," *SIAM Journal on Optimization*, vol. 20, no. 4, pp. 1956–1982, 2010.

[18] R. Otazo, E. Candes, and D. K. Sodickson, "Low-rank plus sparse matrix decomposition for accelerated dynamic mri with separation of background and dynamic components," *Magnetic Resonance in Medicine*, pp. n/a–n/a, 2014.

[19] Gary H. Glover, "Simple analytic spiral k-space algorithm," *Magnetic Resonance in Medicine*, vol. 42, no. 2, pp. 412–415, 1999.

[20] S. Katyal, S. Zughni, C. Greene, and D. Ress, "Topography of covert visual attention in human superior colliculus," *Journal of Neurophysiology*, vol. 104, no. 6, pp. 3074–3083, 2010.

[21] C. Chang and G. H. Glover, "Variable-density spiral-in/out functional magnetic resonance imaging," *Magnetic Resonance in Medicine*, vol. 65, no. 5, pp. 1287–1296, 2011.

[22] J.A. Fessler and B.P. Sutton, "Nonuniform fast fourier transforms using min-max interpolation," *Signal Processing, IEEE Transactions on*, vol. 51, no. 2, pp. 560–574, Feb 2003.